Triggering MSR1 promotes JNK-mediated inflammation in IL-4 activated macrophages

Manman Guo[1#], Anetta Härtlova[1,2#], Marek Gierliński[3], Alan Prescott[4], Josep Castellvi[5], Javier Hernandez Losa[5,6], Brian D. Dill[1], Christoph H. Emmerich[1], Santiago Ramon Y Cajal[5,6], David G. Russell[7] and Matthias Trost*[1,2]

[1]MRC Protein Phosphorylation and Ubiquitylation Unit, University of Dundee, Dundee, UK; [2]Institute for Cell and Molecular Biosciences, Newcastle University, Newcastle upon Tyne, UK;, [3]Data Analysis Group, [4]Division of Cell Signalling and Immunology, School of Life Sciences, University of Dundee, Dundee, Scotland, UK, [5]Department of Pathology, Hospital Universitario Vall d´Hebron, Barcelona, Spain, [6]Spanish Biomedical Research Network Centre in Oncology (CIBERONC), Spain, [7]Department of Microbiology and Immunology, College of Veterinary Medicine, Cornell University, Ithaca, New York, USA

[#]contributed equally.

To whom correspondence should be addressed:
Matthias Trost: Mailing address: matthias.trost@ncl.ac.uk
Institute for Cell and Molecular Biosciences, Medical School, Newcastle University, Newcastle upon Tyne, NE24HH, UK
Tel. ++44 191 2087009

KEY WORDS

Phagocytosis, phagosome, macrophages, Interleukin-4, proteomics, scavenger receptor, MSR1, JNK, Tak1, Mkk7, inflammation, tumour associated macrophages, ubiquitylation, mass spectrometry, lipolysis

RUNNING TITLE

MSR1/JNK signalling in macrophages

ABBREVIATIONS

BMDM, bone marrow-derived macrophages; BSA, bovine serum albumin; ER, endoplasmic reticulum; FDR, false discovery rate; GO, Gene ontology; IFN, interferon; IL-4, interleukin-4; LC, liquid chromatography; LPS, lipopolysaccharide; MS, mass spectrometry; oxLDL, oxidised low-density lipoprotein; ROS, reactive oxygen species; TAMs, tumour-associated macrophages;

Summary

Alternatively activated M2 macrophages (AAMs) play an important role in maintenance of tissue homeostasis by scavenging dead cells and cell debris via phagocytosis. An essential step in this process is phagosomal maturation. Using high-resolution LC-MS/MS, we investigated how alternative activation, driven by IL-4, modulated the phagosomal proteome to control macrophage function. One of the most intriguing insights was the recruitment of the TAK1/MKK7/JNK signalling complex to the phagosomes of IL-4 activated macrophages. The recruitment of this signalling complex was mediated through K63 polyubiquitylation of the macrophage scavenger receptor 1 (MSR1). MSR1 activation induced JNK signalling, thereby facilitating macrophage polarization towards an M1 pro-inflammatory state, which was abolished upon MSR1 deletion or JNK inhibition. Moreover, MSR1 K63 polyubiquitylation correlated with the activation of JNK signalling in ovarian cancer tissue from human patients, suggesting that it may be relevant for macrophage phenotypic shift *in vivo*. Altogether, we identified that MSR1 signals through JNK in a K63-polyubiquitylation-dependent manner and provide evidence for the receptor's involvement in macrophage polarization.

Introduction

Phagocytosis is a highly conserved process essential for host defence and tissue remodelling. It involves the recognition of particles by a variety of cell surface receptors, followed by cargo processing and delivery to lysosomes via phagosome-lysosome fusion, process known as phagosome maturation. This leads to gradual acidification of the phagosomal lumen and acquisition of digestive enzymes required for the degradation of phagosomal cargo. Therefore, phagocytosis is not only responsible for elimination of bacterial pathogens, but also the clearance of apoptotic cells, cell debris and senescence cells and orchestrates the subsequent immune response (Lemke, 2013, Lemke, 2017, Murray & Wynn, 2011, Rothlin et al., 2007). Central to this process is phagosomal maturation. If uncontrolled, the inappropriate clearance of apoptotic bodies can give rise to autoimmune diseases, atherosclerosis and cancer, while failure to ingest or kill pathogens can result in deadly infections (Arandjelovic & Ravichandran, 2015, Colegio et al., 2014, Johnson & Newby, 2009, Nagata et al., 2010). Therefore, it is of great importance to understand which signalling pathways regulate phagocytosis and phagosomal maturation.

It has recently been acknowledged that the phagosome serves as a signalling platform and interacts with innate immune signalling (Heckmann et al., 2017, Kagan, 2012, Martinez et al., 2011, Martinez et al., 2015, Stuart et al., 2007). However, whether phagosome-associated cell signalling is independent of its role in cargo degradation has not been well understood. Supporting this notion, recent proteomic studies demonstrated that phagosomes are dynamic organelles that change their composition and function in response to infection or inflammation (Boulais et al., 2010, Dill et al., 2015, Guo et al., 2015, Hartlova et al., 2018, Naujoks et al., 2016, Trost

et al., 2009). While the regulation of phagosomal maturation in so-called M1 inflammatory macrophages has been extensively studied, the mechanisms facilitating phagosomal maturation in macrophages involved in tissue repair remains poorly understood (Balce DR., Keizer. S.J., 2011)

Th2-derived cytokines, such as interleukin-4 (IL-4) and interleukin-13 (IL-13) induce a strong anti-inflammatory macrophage phenotype, also called alternative activated macrophages (M2). M2 macrophages and tissue resident macrophages, which often resemble an M2-like state, clear cell debris and dead cells through phagocytosis. They are therefore essential for maintenance and tissue homeostasis. M2 alternatively activated macrophages (AAMs) inhibit inflammatory responses and promote angiogenesis and tissue repair by synthetizing mediators required for collagen deposition, which is important for wound healing (Gordon & Martinez, 2010). It has been shown that IL-4 enhanced phagosomal protein degradation (Balce et al., 2011). Whether IL-4 regulates other phagosomal functions, and through which molecular mechanisms, remains unclear.

Here we demonstrate that the TAK1/MKK7/JNK signalling complex showed an enhanced association with the phagosome upon IL-4 macrophage activation using an unbiased quantitative LC-MS/MS approach. We further show that the assembly of the signalling complex is mediated through K63 polyubiquitylation. By combining K63-polyubiquitylation enrichment and mass spectrometry approaches, we identified macrophage scavenger receptor 1 (MSR1) as the upstream receptor that promotes the recruitment of the TAK1/MKK7/JNK signalling complex to the phagosome. Triggering MSR1 induces JNK activation in M2 macrophages. This MSR1/JNK signalling pathway activation leads to a M2/M1 macrophage phenotypic switch that is abolished

in macrophages lacking MSR1. We demonstrate that MSR1 is K63 ubiquitylated and signals through JNK in human patient ovarian cancer, thus suggesting a potential role in human cancer.

Results

Alternative activation regulates phagosomal proteolysis and lipolysis

To determine the impact of IL-4 on phagocytosis and phagosomal functions, we examined the rate of phagocytosis and phagosomal maturation in IL-4 AAMs (M2) and resting macrophages (M0). We found that M2 macrophages have enhanced uptake of apoptotic cells, while uptake of necrotic cells was comparable to M0 resting macrophages (**Figure 1A**). To determine whether the enhanced uptake was because of the negative charge of apoptotic cells, we compared the uptake of fluorescently-labelled carboxylated negatively charged and amino positively charged silica microsphere in M2 and M0 macrophages. The analysis revealed an increased uptake of negatively charged microspheres in M2 macrophages, while the engulfment of positive charged microsphere was similar to M0 macrophages indicating a similarity of carboxylated microspheres with apoptotic cells (**Figure 1B**). Next we analysed the functional parameters of the phagosomal lumen including proteolysis, acidification and lipolysis using real-time fluorescence assays (Podinovskaia et al., 2013, Yates et al., 2005). Consistent with the previous reports, we observed enhanced proteolytic activity in phagosomes of M2 macrophages (Balce et al., 2011). Furthermore, we found that IL-4 increased phagosomal lipid degradation and facilitated phagosomal acidification (**Figure 1C-E**) indicating that IL-4 activation promotes ability of macrophages to degrade lipid-rich particles through phagosomes.

Quantitative proteomics analysis of phagosomes from IL-4 alternatively activated macrophages

To obtain further molecular details about the changes on phagosomes of M2 macrophages, we isolated highly pure phagosomes from M2 and M0 macrophages by floatation on a sucrose gradient using carboxylated microspheres and analysed their proteomes by quantitative LC-MS/MS (**Figure 1A, S2A**) (Desjardins et al., 1994, Trost et al., 2009). Comparative analysis led to the identification of 20,614 distinct peptides corresponding to 1,948 unique proteins across three independent replicates at a false-discovery rate (FDR) of <1%, of which 1,766 proteins were quantified in at least two of the three biological replicates. IL-4 activation induced strong changes to the phagosome proteome with 121 proteins significantly up- and 62 proteins significantly down-regulated (2-fold change, $p<0.05$) (**Figure 2B; Table S1**), some of which we validated by Western blot analysis (**Figure S2B**). Consistent with the above observations, a subset of proteins involved in lipid metabolism (Lpl lipoprotein lipase, ABHD12 lipase and phospholipase D1), acidification (v-ATPase complex) and lysosomal enzymes including cathepsins L1 and D were highly enriched on the phagosome of M2 macrophages (**Figure 2D, Table S1**). Moreover, GO-term (**Figure 2E**) and protein network analysis (**Figure S2C**) further showed that IL-4 alternative activation also increased phagosome abundance of scavenger receptors such as MARCO, CD36, Colec12 and MSR1 required for clearance of dead cells while Toll-like receptors (TLRs) involved in inflammatory response were reduced (**Figure 2E, S2C**). Consistent with previous report, superoxide anion generation including the NADPH oxidase complex proteins NCF1 (p47-phox), Cyba (p22-phox), Cybb (gp91-phox) and superoxide dismutase SOD1 were strongly down-regulated in phagosomes from M2 macrophages (**Figure 2E, Figure S2C)** (Balce et al., 2011). Interestingly, M2 macrophages also enriched a large number of specific carbohydrate-binding proteins such as lectins,

while carbohydrate hydrolases were significantly reduced. This indicates a conservation of phagocytosed glycans, potentially for antigen presentation via MHC class II molecules (Avci et al., 2013). Furthermore, M2 phagosomes showed higher phosphatidylinositol-binding proteins, suggesting changes to the phagosome membrane lipid content. Taken together, these results indicate that the phagosome of M2 macrophages has mainly a homeostatic role with its increased ability to hydrolyse proteins and lipids of incoming cargo.

TAK1/MKK7/JNK are recruited to the phagosome of M2 macrophages via K63 polyubiquitylation

Interestingly, anti-inflammatory IL-4 activation also led to an increased phagosome abundance of the pro-inflammatory MAP-kinase signalling complex around TAK1 (Map3k7, 2.1-fold) and MKK7 (Map2k7, 3.1-fold) (**Table S1, Figure S2C)** indicating cross-regulation between anti- and pro-inflammatory pathways. Given the increased abundance of these pro-inflammatory kinases was surprising on phagosomes of IL-4-stimulated macrophages, we next investigated how this complex was translocated to the phagosome. Immunoblot analyses of total cell lysates and phagosomal fractions revealed significant enrichment of TAK1 and MKK7 on phagosomes of M2 macrophages compared to resting M0 macrophages (**Figure 3A, B**). Activated TAK1 can phosphorylate two MAPK kinases, MKK4 and MKK7, both implicated in the activation of JNK. While MKK4 can activate p38 and JNK MAPKs signalling pathways, MKK7 selectively activates JNK (Tournier et al., 2001). Noteworthy, our mass spectrometry data revealed that only MKK7 was enriched on phagosomes upon IL-4 alternative activation. Consistent with our LC-MS/MS data, MKK4 was not detected on

phagosomes of M2 macrophages by immunoblot analysis indicating that MKK7 alone was important in this phagosome signalling pathway. Further immunoblot analysis also confirmed enrichment of JNK of M2 macrophage phagosomes.

Previous data have shown that upon pro-inflammatory Interleukin-1 receptor or Toll-like receptor (TLR) activation, the TAK1/MKK7/JNK complex binds to the TAB1/TAB2 protein complex, which in turn is recruited to K63 polyubiquitin chains (Emmerich et al., 2013, Xia et al., 2009). We next tested whether TAB1/TAB2 are recruited to the phagosome of M2 macrophages. Indeed, immunoblot analysis demonstrated enrichment of TAB1/TAB2 on phagosomes of M2 macrophages compared to M0. To further validate the recruitment of the protein complex to phagosomes, we performed confocal fluorescence microscopy and showed vesicular distribution in the cytoplasm with enhanced recruitment of TAB1, TAB2 and MKK7 to the M2 macrophage phagosome compared to M0 macrophages (**Figure S3A-B**).

As it is well-established that TAK1 binds via TAB1/2/3 to free and protein-anchored K63-polyubiquitin chains in inflammatory innate immune responses (Emmerich et al., 2013, Xia et al., 2009), we tested whether phagosomes from M2 macrophages contain K63-polyubiquitylated proteins independent of inflammatory stimuli. Immunoblot analysis of phagosome extracts probed with anti-K63 polyubiquitin antibodies revealed that phagosomes contain a large amount of K63-polyubiquitylated proteins compared to the total cell lysate, which was even more increased by alternative activation (**Figure 3C**). To determine whether recruitment of TAB1, TAB2, TAK1 and MKK7 to the M2 phagosome was indeed K63 polyubiquitylation-dependent, we treated cells with NSC697923, a pharmacological inhibitor of the K63-specific E2 conjugating enzyme UBC13-UEV1A (Pulvino et al.,

2012) and probed isolated phagosomes for K63 polyubiquitylation. As shown in **Figure 3D**, recruitment of the protein complex was virtually abolished under these conditions. These data indicate that IL-4 activation of macrophages promotes K63 polyubiquitylation which recruits the TAK1/MKK7/JNK complex to the phagosome.

Macrophage scavenger receptor 1 is K63 polyubiquitylated and interacts with TAK1/MKK7/JNK on the phagosome of M2 macrophages

To identify the K63 polyubiquitylated associated with TAK1/MKK7/JNK complex on the phagosome of M2 macrophages, we enriched polyubiquitylated phagosomal proteins from M2 macrophages using tandem ubiquitin-binding entities (TUBEs) of a repeat of the Npl4 Zinc Finger (NZF) domain of TAB2 tagged with Halo (termed here Halo-TAB2) that bind to K63 polyubiquitin chains (**Figure 4A**) (Emmerich et al., 2013, Heap et al., 2017, Hjerpe et al., 2009). Quantitative mass spectrometric analysis of these pull-downs identified 538 proteins that were reproducibly captured by Halo-TAB2 compared to mutant Halo [T674A/F675A] TAB2 control beads (based on a 2-fold, $p<0.05$ cut-off) (**Table S2**). Moreover, we identified 62 novel direct ubiquitylation (-GlyGly) sites on 33 different proteins. Quantitation of the data revealed that the Gly-Gly peptide derived from K63-linked polyubiquitin was by far the most abundant, proving that we achieved good enrichment. However, we also identified peptides for K11, K48 , linear/M1, K29, K6, K27 and K33 (in order of decreasing abundances) linked polyubiquitin, suggesting that there are either mixed chains or K63-polyubiquitylated proteins might also be modified with other polyubiquitin chains.

Other identified ubiquitylated proteins included many known phagolysosomal proteins such as the large neutral amino acid transporter SLC43A2/LAT4 (K283, K293, K402, K557), the cholesterol transporter ABCG1 (K55), Fc- and B-cell Receptor adaptor LAT2 (K39, K84), LYN kinase (K20) and the TLR chaperone UNC93B1 (K197, K582) (**Figure 4B, Table S3**).

Interestingly, one of the most abundant Gly-Gly-modified peptides was a peptide containing lysine 27 (K27) of macrophage scavenger receptor 1/scavenger receptor A (MSR1/SR-A; CD204). This site is highly conserved between human and mouse (**Figure 4C**). MSR1 is a multifunctional phagocytic receptor, highly expressed in macrophages, involved in uptake of apoptotic cells and modified lipoproteins (Kelley et al., 2014). In addition to its scavenging function, MSR1 has been implicated in the innate immune response to bacteria (Platt & Gordon, 2001).

Our MS and immunoblot data showed an increase of MSR1 on phagosomes from M2 macrophages compared to M0 macrophages **(Table S1, Figure S4A)**, while both total cell and cell surface expression levels of MSR1 were unchanged between the two conditions (**Figure S4B**). However, when we precipitated K63-polyubiquitylated proteins from resting and M2 macrophages, we could see that the polyubiquitylated forms of MSR1 were considerably more abundant in alternatively activated macrophages (**Figure 4D**), suggesting that MSR1 becomes polyubiquitylated in M2 macrophages.

To validate K63 polyubiquitylation of MSR1, we treated enriched polyubiquitylated phagosome protein extracts from M2 macrophages with the K63-specific deubiquitylase (DUB) AMSH-LP or the non-specific DUB USP2 (Ritorto et al., 2014) (**Figure 4E**). In both cases, the high molecular smear of ubiquitylated MSR1

decreased while the band representing the non-ubiquitylated form of MSR1 increased significantly, indicating that MSR1 was predominantly K63 polyubiquitylated on phagosomes upon uptake of carboxylated beads in M2 macrophages.

We next investigated whether K63-polyubiquitylated MSR1 might recruit the TAB1/TAB2/TAK1/MKK7 complex to the phagosome. To test this, we pulled down MSR1 from extracts of carboxylated bead phagosomes. We found that indeed TAB1/TAB2/TAK1/MKK7 complex co-immunoprecipitated with MSR1 (**Figure 4F**). Moreover, using a different antibody against TAK1, immunoblot analysis patterns indicated also substantial post-translational modification – most likely polyubiquitylation - of TAK1, which was considerably enhanced in MSR1 IPs. It has been reported that ubiquitylation of TAK1 activated the kinase activity (Fan et al., 2010), suggesting that TAK1 and the downstream kinase MKK7 are recruited in the active state or activation is triggered by binding to K63 polyubiquitylated MSR1. Taken together, these data demonstrate that MSR1 becomes K63 polyubiquitylated upon activation in IL-4-activated macrophages which recruits the TAK1/MKK7 kinase signalling complex.

Triggering MSR1 activates JNK pathway

To further test whether the engagement of MSR1 causes the activation of the TAK1/MKK7/JNK pathway, wild-type (WT) and MSR1 KO M2 macrophages were stimulated with the MSR1 ligands fucoidan and oxidized LDL (oxLDL) and analysed for MSR1 K63-polyubiquitylation and activation of JNK signalling (Greaves & Gordon, 2009). The analysis revealed that M2 macrophages deficient in MSR1 showed diminished MSR1 K63-polyubiquitylation and decreased JNK phosphorylation upon

fucoidan or ox-LDL stimulation (**Figure 5A**, **5B**), indicating that MSR1 directly signals through the JNK signalling pathway. This prompted us to test whether MSR1-signalling through the JNK kinase complex plays a role in affecting the inflammatory state of macrophages by characterizing gene expression and cell surface markers. Ablation of MSR1 resulted in diminished induction of the pro-inflammatory genes *Il1b* and *Tnfa* in response to fucoidan in M2 macrophages. Consistently, MSR1 KO M2 macrophages exhibited reduced cell surface expression of pro-inflammatory markers CD69, CD86 and CD54 while CD36, M2-cell surface marker, remained unperturbed upon MSR1 ligation (**Supplementary Figure S5A, B**). This increase in pro-inflammatory state was abolished by treatment with the specific JNK inhibitor JNK-IN8 (Zhang et al., 2012) (**Figure 5D, E, Supplementary Figure S5B, C**). This process was dependent on specific MSR1 ligands as stimulation with Toll-like receptor 4 (TLR4)-activating Lipopolysaccharide (LPS) and IFN-γ did not show any differences between WT and MSR1 KO macrophages (**Figure S5A**) suggesting the involvement of MSR1-JNK pathway in phenotypic switch. These data show that triggering of MSR1 in alternatively activated macrophages leads to the enhanced activation of the JNK signalling pathway, which induces a pro-inflammatory phenotype switch in these macrophages.

MSR1 is polyubiquitylated in human tumour associated macrophages

Next, we wanted to test if MSR1 ubiquitylation was also present in settings of human disease. MSR1 has been implicated in tumour development and progression (Chanmee et al., 2014, Komohara et al., 2009) and tumour-associated macrophages (TAMs) have been shown to resemble M2 macrophage phenotype with MSR1 protein expression (Sica et al., 2007). However, the role of MSR1 in TAMs is not fully

understood. We characterised five human patient samples with different types of cancers for the presence of MSR1. These tissue samples showed a high variability in the number of TAMs that stained positively for MSR1 using immunohistochemistry (**Figure 6A**). Consistent with the human proteome atlas data (http://www.proteinatlas.org/ENSG00000038945-MSR1/cancer), we found particularly high expression of MSR1 in patient ovarian cancer. Interestingly, the TAMs of the patient with ovarian cancer also showed increased levels of ubiquitylated MSR1 as well as enhanced phosphorylation of JNK and its substrate c-Jun (**Figure 6B**). This suggests that JNK signalling downstream of poly-ubiquitylated MSR1 is present in TAMs of human cancers and could potentially be involved in tumour promotion.

Discussion

Macrophages are highly diverse and plastic immune cells that can polarise in response to environmental cues into many different phenotypes. Because of their important and diverse functions in regulating immune responses and metabolism, dysregulated macrophage polarization is frequently associated with disease (Schultze et al., 2015). Here we expand our understanding of macrophage phenotype switching by showing on the molecular level that engagement of MSR1 in IL-4-activated macrophages results in the activation of the JNK signalling pathway, thereby inducing a shift from an anti-inflammatory to a proinflammatory phenotype.

Recent data implies that distinct pathways regulate uptake kinetics of different particles as well as phagosome functions in macrophages and these are further controlled by macrophage activation. It was demonstrated that both the phagocytic receptors (Balce et al., 2016, Dill et al., 2015) and pro-inflammatory (Ghigo et al.,

2010, Trost et al., 2009, Yates et al., 2007) and anti-inflammatory activation (Balce et al., 2011, Varin et al., 2010) of macrophages affects phagosome functions and these are regulated by signalling pathways such as kinases (Hartlova et al., 2018) and E3-ligases (Bilkei-Gorzo et al., *unpublished data*).

A striking finding from our study is the identification of increased ubiquitylation on the phagosome. Ubiquitylation in the endo-lysosomal system is generally thought to be important for lysosomal degradation of membrane proteins (Piper et al., 2014). Our data indicates that K63-polyubiquitylation on phagosomal proteins is also used as a scaffold for the recruitment of signalling complexes, in particular the kinase complex TAK1/MKK7/JNK to MSR1 via specific polyubiquitylation on a conserved lysine K27. Remarkably, we could show that only MKK7 and not MKK4 is recruited to this signalling complex in IL-4-activated macrophages, showing a different role for the two MAP kinase kinases in activating JNK.

It is noteworthy that MSR1 is in almost equal abundance in resting, alternatively and classically activated macrophages. This indicates that macrophage activation (as signal 1) induces activation or transcription or translocation of an E3 ligase. This unknown E3 ligase then ubiquitylates, after MSR1 ligation (signal 2), the receptor, enabling proinflammatory signalling through the TAK1/MKK7/JNK signalling complex (**Figure 6C**). During inflammation, this signalling probably does not add substantially to the macrophage phenotype as TLR or IL1R activation induces a much stronger pro-inflammatory signal. However, in M2 or tissue-resident macrophages with a similar M2-like phenotype, prolonged MSR1 ligation could lead to a pro-inflammatory switch of these macrophage subsets via JNK. Interestingly, recent data in Drosophila showed that apoptotic corpses prime macrophages for detection of

tissue damage and that this priming and subsequent recruitment to wounds was dependent on JNK (Weavers et al., 2016). This suggests that JNK activation induced by uptake of apoptotic bodies could regulate various responses.

MSR1 has in recent years been established as a good marker for TAMs (Allavena & Mantovani, 2012) which resemble rather a M2 alternatively activated phenotype and have been associated with tumour promotion (Sica et al., 2007). While previously it was shown that lack of MSR1 delayed the growth of EL4 lymphoma in mice by increased pro-inflammatory responses to necrotic cells (Komohara et al., 2009), our data revealed an increased expression of K63-polyubiquitylated MSR1 in a human ovarian cancer. This coincided with increased activation of JNK pro-inflammatory signalling pathway, suggesting that the MSR1-JNK signalling pathway is activated in the progression of cancer. Interestingly, MSR1 has been previously shown to promote tumour progression and metastasis in ovarian and pancreatic cancer mouse models (Neyen et al., 2013), suggesting that MSR1 and downstream signalling may be a potential drug target in the prevention of cancer metastasis progression.

Methods

Antibodies

The following antibodies were purchased from Cell Signalling Technology: pSTAT1 (#8826), Arginase-1 (#9819), Rab7 (#9367), Rab5 (#2143), BIP (#3183), EEA1 (#2411), LAMP1 (#3243), Na^+/K^+ ATPase 1 (#3010), Lamin A/C (#2032), TAK1 (#4505), JNK (#9258), p-JNK (#9251), p-cJUN (#9165) and Vimentin (#5741). Antibodies purchased from Abcam were: pSTAT6 (ab54461), CD36 (ab133625), CD14 (ab182032) and MSR1 (ab151707, ab79940). Antibodies against K63-specific Ubiquitin (#05-1308) and ITGAM (PAB12135) were from Millipore and Abnova, respectively. Sheep antibodies against MSR1, TAK1, TAB1, TAB2, MKK7 and MKK4, and rabbit IgG were generated by the Antibody Production Team of the Division of Signal Transduction Therapy (DSTT), Medical Research Council Protein Phosphorylation and Ubiquitylation Unit, University of Dundee, United Kingdom. The antibody used for MSR1 immunohistochemistry was clone SRA-E5 (from Abnova, #MAB1710). Commercial antibodies were used according the manufacture instructions. DSTT-made antibodies were used at 2 µg/ml in TBS-T containing 5% non-fat dried milk. Recombinant proteins, plasmids and antibodies generated for the present study are available to request on our reagents website (https://mrcppureagents.dundee.ac.uk/).

Culturing and activation of bone marrow-derived macrophages

Bone marrow cells were collected from femurs and tibiae of 6–8 week old C57BL/6 wild type (WT) or MSR1/SR-A knock-out mice (kindly provided by Siamon Gordon). The cells were treated with red blood cell lysis buffer (155 mM NH_4Cl, 12 mM $NaHCO_3$,

0.1 mM EDTA) and plated on tissue culture plastic (Corning Incorporated) for 3 days in DMEM (Gibco) containing 10% FBS, 2 mM glutamine, 100 units/ml Penicillin-Streptomycin (Gibco), and 20% L929 conditioned supplement. At day three, the cells in supernatant were transferred to untreated 10 cm Petri dishes (BD Biosciences) for seven days for the differentiation into bone marrow-derived macrophages (BMDMs). Then, BMDMs were treated by either IL-4 (20 ng/ml, BD Pharmingen) for 48 h to get M2(IL-4) Macrophages (**Figure S1**).

Phagosome isolation

For proteomic analysis, phagosomes were isolated from BMDMs according to previous methods (Desjardins et al., 1994, Trost et al., 2009). Latex beads of 0.8 µm (Estapor/Merck, Fontenay Sous Bois, France) were diluted 1:50 in complete DMEM media and incubated with treated and untreated BMDMs for 30 min at 37 °C, 5% CO_2. Cells were then harvested on ice, washed in cold PBS, and phagosomes were isolated as described in previous works (Guo et al., 2015, Trost et al., 2009). Enriched protein extracts contained less than 5% contamination from other cellular organelles as estimated from immunoblotting experiments (**Figure S2A**).

For pull down assays, phagosomes were isolated using 1 µm magnetic beads (Estapor/Merck). Magnetic beads were diluted 1:300 in complete DMEM media and incubated with BMDMs for 30 min.

Phagosome functional assays

Fluorogenic assays for phagosomal proteolysis, acidification and lipolysis were adapted from the method from the Russell laboratory (Podinovskaia et al., 2013,

VanderVen et al., 2010, Yates et al., 2005). For proteolysis and acidification BMDMs were plated onto 96-well plates at 1 × 10^5 cells per ml 24 h prior to the experiment. DQ red BSA (Life Technologies) -coupled or BCECF (Life Technologies) -coupled carboxylated silica beads (3 µm, Kisker Biotech) were diluted 1:200 in binding buffer (1 mM $CaCl_2$, 2.7 mM KCl, 0.5 mM $MgCl_2$, 5 mM dextrose, 10 mM hydroxyethyl piperazine ethane sulfonate (HEPES) and 5% FBS in PBS pH 7.2) and incubated with BMDMs for 3 minutes at room temperature. Beads were replaced with warm binding buffer, and real-time fluorescence was measured at 37°C using a SpectraMax Gemini EM Fluorescence Microplate Reader (Molecular Devices), set as maximal readings per well to allow reading time intervals of 2 minutes. Plots were generated from the ratios of signal/control fluorescence. For lipolysis, Nucleosil 120-3 C18 reverse phase HPLC 3 µm silica matrix were coated with a mixture of neutral lipids containing a fluorogenic substrate specific to detect the lipase activity and a calibration fluorogenic dye. Substrate-labelled beads were incubated with BMDMs on coverslips for 3 min at room temperature. The coverslips were then washed and loaded into quartz cuvettes in binding buffer. Fluorescent intensities were recorded in real time at 37°C with a thermostat-regulated QMSE4 spectrofluorometer (Photon Technologies International, Lawrenceville, NJ, USA) with excitation/emission 342/400 nm for reporter dye and 555/610 nm for calibration dye.

Phagocytosis assays

Phagocytosis of beads was performed by incubating Alexa Flour 488 BSA-coated silica beads at 1:1000 dilution with BMDMs in 96-well plates for 10 min at 37 °C. Beads were replaced with 100 µl trypan blue to quench the fluorescence of non-internalised

particles. After aspirating trypan blue, the fluorescence was measured in a SpectraMax Gemini EM Fluorescence Microplate Reader, set at excitation/emission wavelengths 495/519 nm.

Uptake of apoptotic/necrotic cells

Uptake of apoptotic or necrotic cells was performed as follows: GFP-expressing RAW264.7 cells were induced apoptosis by 50 µM cycloheximide for 24 h or necrosis by repeated *freeze*/*thaw* cycles. Both apoptotic and necrotic cells were vigorously washed in PBS and then added to BMDMs for 6 h at 37°C, in a phagocyte to target ratio of approximately 1:5. The percentage of BMDMs that had interacted with apoptotic cells was quantified by FACS analysis of AF488 positive cells. A minimum of 50,000 events within the macrophage gate was acquired.

Sample preparation and mass spectrometry analysis

Phagosome proteins were extracted using 1% sodium 3-[(2-methyl-2-undecyl-1,3-dioxolan-4-yl)methoxy]-1-propanesulfonate (commercially available as RapiGest, Waters) in 50 mM pH 8.0 Tris, reduced with 1 mM tris(2-carboxyethyl)phosphine (TCEP), and alkylated by 5 mM iodoacetamide (30 min, room temperature, in the dark) (Sigma) and then quenched by 10 mM DTT. Protein concentrations were determined using EZQ protein quantitation kit (Life Technologies). Samples were then diluted in 50 mM Tris containing 5 mM calcium chloride to a final concentration of 0.1% RapiGest, and were digested by Trypsin Gold (Promega). RapiGest was removed by adding trifluoroacetic acid (TFA) to 1%, shaking at 37 °C for 1 h and centrifugation at 14,000 xg for 30 min. Peptides were desalted by solid phase extraction using

Microspin C-18 (Nest Group), lyophilised and labelled using mTRAQ labelling kit (Δ0 and Δ8 Da; AB-Sciex) for phagosomal samples.

Mass spectrometric analyses were conducted similarly as previously described (Dill et al., 2015, Guo et al., 2015). In detail, biological triplicates or quadruplicates of mixes of 1 µg of light-labelled and 1 µg of heavy-labelled samples were analysed on an Orbitrap Velos Pro mass spectrometer coupled to an Ultimate 3000 UHPLC system with a 50 cm Acclaim PepMap 100 or EasySpray analytical column (75 µm ID, 3 µm C18) in conjunction with a Pepmap trapping column (100 µm x 2 cm, 5 µm C18) (Thermo-Fisher Scientific). Acquisition settings were: lockmass of 445.120024, MS1 with 60,000 resolution, top 20 CID MS/MS using Rapid Scan, monoisotopic precursor selection, unassigned charge states and z=1 rejected, dynamic exclusion of 60s with repeat count 1. Six hour linear gradients were performed from 3% solvent B to 35% solvent B (solvent A: 0.1% formic acid, solvent B: 80% acetonitrile 0.08% formic acid) with a 30 minute washing and re-equilibration step.

Proteome quantification and bioinformatics analysis

The phagosome proteomics dataset of IL-4-activated macrophages was extracted from a combined analysis of phagosomes from five different activations states (IL-10, IL-13, IFN-γ and IFN-γ+IL-4; PRIDE identifier PXD004520). Only proteins identified and quantified in the IL-4-treated dataset were extracted from this. Identification and quantification was performed using MaxQuant v1.3.0.5 (Cox & Mann, 2008) with variable modifications Oxidation (M), Acetyl (Protein N-term), Deamidation (NQ), 2 multiplicities with mTRAQ Lysine/N-terminal (Δ0 and Δ8) (for phagosome samples) or label-free and Gly-Gly (K) (for TUBE samples), maximum 5 modifications per peptide,

and 2 missed cleavages. Spectra were matched to a Uniprot-Trembl *Mus musculus* database (50,543 entries, downloaded October 18, 2012) plus common contaminants. A reverse database was used for false peptide discovery. Mass accuracy was set to 10 ppm for precursor ions and 0.5 Da for ion trap MS/MS data. Identifications were filtered at a 1% false-discovery rate (FDR) at the protein and peptide level, accepting a minimum peptide length of 7. Quantification used only razor and unique peptides, and required a minimum ratio count of 2. “Re-quantify” and “match between runs” were enabled. Normalized ratios were extracted for each protein/condition and used for downstream analyses.

Statistical analyses were performed in Perseus (v1.3.0.4). T-test-based statistics were applied on normalized and logarithmized protein ratios to extract the significant regulated proteins. Hierarchical clustering was performed in Perseus on logarithmized ratios of significant proteins using Correlation distances and Average linkage to generate the heatmap.

GO term and Network analyses

The H/L log fold changes for all quantifiable proteins in each condition (in replicates) were tested against the null hypothesis that the mean log fold change was zero. We used a one-sample t-test with shrinkage variance of Opgen-Rhein & Strimmer (Opgen-Rhein & Strimmer, 2007). Each protein was annotated with GO-terms from Mouse Genome Informatics Database (downloaded on 5/11/2014). Log fold change of each GO-term was calculated as the mean of log fold changes of all proteins annotated with this GO-term. The significance of this mean, against the null hypothesis that the mean is zero (i.e., there is no discernible fold change in the GO-term proteins), was found

using a bootstrap technique. A protein sample of the same size as the GO-term group was randomly selected (without replacement) from the pool of all quantifiable proteins and its mean log fold change found. The sampling process was repeated 100,000 times and the significance p-value was determined as the percentile of bootstraps where the absolute log fold change was greater than in the GO-term group. Proteins annotated with given GO-terms are presented in 'volcano plots', showing, for each protein, the mean log fold change of replicates versus the p-value. The error bars represent the shrinkage standard error.

Protein networks were extracted from STRING database v10 (Szklarczyk et al., 2015) using only "experiment" and "text-mining" data. Graphs were generated using Cytoscape v3.3 (Shannon et al., 2003).

Immunonoblot analysis

Cells or phagosomes were lysed directly in 2x Laemmli buffer, separated on 4-12% Nu-PAGE gels (Invitrogen) and immunoblotted onto PVDF membranes (Amersham). Membranes were blocked for 1 hr in 5% (w/v) skim milk in TBS containing 0.1% (v/v) Tween 20 and subsequently incubated with different primary antibodies overnight. After incubation with HRP-labeled secondary antibodies, proteins were detected using ECL and X-ray films. Immunoblots were quantified in ImageJ software.

Immunofluorescence

Resting and alternative-activated BMDMs were seeded at 1 × 10^5/ml on glass coverslips. Silica beads (3 µm, Kisker Biotech) were phagocytosed for 30 min by using a dilution of 1:1000 in cell culture media. Cells were subsequently fixed in 4% paraformaldehyde (Affymetrix) and permeabilized by incubating for 5 min with PBS

containing 0.02% NP-40. Rabbit anti-Rab7a antibody was used at dilution of 1:300 to indicate the phagosomes. To visualize the phagosomal location of interested proteins, sheep anti-TAK1/TAB1/TAB2/MKK7 antibodies (DSTT) were used at 4 µg/ml. Cells were imaged in a Zeiss LSM 700 confocal microscope using a x100 Plan Apochromat objective (NA 1.46) and an optical section thickness of 0.7 µm. For quantitation, all laser, pin-hole and gain, etc. settings kept the same for all images. Fields of cells were selected at random using only the DAPI stained channel. Optical sections were taken through the centre of the cell including the beads and 10 fields collected per coverslip. A region of interest (ROI) was drawn around each bead-containing phagosome, the Rab7a ring associated with the bead was included. The green intensity was collected for the same ROI. The integrated sum of the red and green intensities in each ROI were collected and expressed as a ratio. At least 25 individual phagosomes were analysed for each protein target. DAPI, Green-Alexa 488 (target antigen), Red-Alexa 594 (Rab7a) and DIC channels were all collected and images were quantified using the Volocity programme (Perkin-Elmer).

TUBE-pull down

Phagosomes were isolated from M2(IL-4) macrophages using magnetic beads. Phagosomal proteins were solubilized in cell lysis buffer (50 mM Tris/HCl pH7.5, 1 mM EGTA, 1mM EDTA, 1% Triton X100, 0.27 M sucrose, 0.2 mM PMSF, 1 mM benzamidine), plus 1% SDS and inhibitors of proteases, phosphatases and deubiquitylases were added freshly. Cell lysates were clarified by centrifugation at 14,000 xg for 30 min at 4°C. The supernatants were collected and their protein concentrations were determined by EZQ protein quantitation kit. For each pull down,

500 µg of phagosome lysate was diluted in cell lysis buffer to make a final concentration of 0.1% SDS, and then incubated with Npl4 Zinc Finger (NZF) domains of TAB2 (TAB2[644-692]) coupled beads, which were previously described (Emmerich et al., 2013). Ubiquitin binding-defective mutant TAB2 (T674A/F675A)-beads were included as negative control. After overnight incubation at 4°C , the beads were washed three times with 50 mM Tris/HCl, pH 8.0, 0.5 M NaCl, 1% Triton X-100 and eight times with 50 mM Tris/HCl, pH 8.0. Captured proteins were then eluted by incubation for 15 min with 50 mM Tris/HCl, pH 8.0, 1% RapiGest, and 5 mM TCEP and centrifugation at 1,000 xg for 5 min.

Deubiquitylation assay

The polyubiquitylated proteins captured by Halo-TAB2 beads were washed twice in reaction buffer (50 mM Tris pH 7.5, 50 mM NaCl, 2 mM DTT). The beads were then incubated with or without AMSH-LP (5 µM) or USP2 (1 µM) in 30 µl reaction buffer at 30 °C for 1 h. The reaction was quenched by denaturation in 1% LDS. Eluted proteins were separated on SDS-PAGE and immunoblotted with anti-MSR1 or anti-K63 pUb chain antibodies.

MSR1 co-immunoprecipitation from phagosome extracts

Rabbit anti-MSR1 antibody and rabbit IgG were coupled to protein A-Sepharose (Amersham Biosciences) by incubation in PBS for 5 h at 4 °C. Then antibodies were cross-linked to the Sepharose by incubating with 20 mM dimethyl pimelimidate dihydrochloride (DMP, Sigma) in 0.1 M sodium tetraborate decahydrate (Sigma) pH 9.3 for 30 min at room temperature. Excess antibody was removed by washing the

sepharose in 50 mM glycine (Sigma) pH 2.5. The resin was washed extensively with 0.2 M Tris-HCl pH 8.0. Phagosomes were isolated from M2(IL-4) macrophages using magnetic beads. Phagosomal lysate of 500 µg was incubated with antibody cross-linked Sepharose in cell lysis buffer for 5 h at 4 °C. The beads were washed three times with 1 ml of lysis buffer. Immunoprecipitated proteins were eluted by denaturation in 1% LDS and subjected to immunoblotting.

Preparation of oxLDL

Human low-density lipoprotein (Millipore) was oxidised by incubating at 1 mg/ml with 5 µM $CuSO_4$ (Sigma) in PBS for 18 h at 37 °C. The oxidised low-density lipoprotein (oxLDL) was dialysed in a dialysis cassette (Pierce) against PBS to remove $CuSO_4$, and then added to BMDMs at the desired concentration.

Quantitative real-time PCR

RNA was isolated from cells using RNeasy kit from Qiagen. Total RNA (500-1000 ng) was used to synthesize cDNA with the QuantiTect Reverse Transcription Kit (Qiagen). Quantitative real-time PCR analysis was performed using the iTaq™ Universal SYBR® Green Supermix and analyzed using the CFX384 Touch™ Real-Time PCR Detection System (Bio-Rad). The results were normalized to *Gapdh* and expressed as fold change relative to RNA samples from control or mock-treated cells using the comparative CT method ($_{\Delta\Delta CT}$). The following validated QuantiTect primer assays (Qiagen) were used: *Gapdh, Il1b, Tnfa.*

Flow cytometry analysis

M0 and M2(IL-4) were incubated with fucoidan from *Fucus vesiculosus* (50 µg/ml; Sigma-Aldrich) and oxLDL (50 µg/ml) for 24 h, after which cells were collected at 1 × 10^6 cell per tube into polystyrene tubes (Corning Incorporated). Cells in each tube were washed twice in PBS/FBS (1% FBS in PBS, pH 7.2) by centrifugation at 1,200 xg for 3 min and resuspended in 100 µl blocking buffer (1 to 50 dilution of CD16/CD32 in PBS/FBS) to block Fc receptors. Following 15 min incubation in ice, cells were washed once in PBS/FBS and then incubated with 100 µl PBS/FBS containing 1 to 100 dilution of phycoerythrin (PE)-conjugated CD54, CD69, CD86, CD301b or CD36 antibodies (eBioscience) for 30 min on ice, respectively. PE-CD11b (eBioscience) was mixed with each antibody at 1 to 200 dilution as control. After washing for three times in PBS/FBS, cells were analysed by flow cytometry.

JNK inhibitor treatment

BMDMs were pre-treated with 0.3 µM JNK7 or JNK8 inhibitor (Zhang et al., 2012) 1 h before stimulation with 50 µM of Fucoidan for the indicated time (6 h – RT-PCR analysis, 24 h – FACS analysis).

Immunohistochemistry

Three micrometer tissue sections from selected paraffin blocks of primary human tumours were prepared. Slides were incubated overnight at 56°C, deparaffinized in xylene for 20 min, rehydrated through a graded ethanol series, and washed with PBS. Immunohistochemistry was performed on a Ventana Benchmark XT automatic immunostaining device (Roche). A heat induced epitope retrieval step was performed

in Ventana CC1 solution for 60 minutes. Primary antibodies were incubated for 40 minutes, 60 minutes and 120 minutes, respectively. An Ultravision detection system was used.

Data availability

Mass spectrometric raw data are available through the PRIDE repository (https://www.ebi.ac.uk/pride/archive/) and have been assigned the identifiers PXD010478 (TUBE data; **Username:** reviewer61442@ebi.ac.uk **Password:** GDRWhOkY) and PXD004520 (phagosome proteomics data; **Username:** reviewer26301@ebi.ac.uk **Password:** PSZ2j2Kz).

Statistical analysis

Statistical analysis was performed using GraphPad Prism software. Definition of statistical analysis and *post hoc* tests used can be found in figure legends. The statistical significance of data is denoted on graphs by asterisks (*) where $*P < 0.05$, $**P < 0.01$, $***P < 0.001$ or ns = not significant.

Author contributions

MGu and AH performed most experiments; AP, JC, JHL, BD, CHE and DGR performed additional experiments; MGu, MGi and MT performed data analysis; SRC and DGR provided intellectual input; MT, AH and MGu designed experiments; MT, AH and MGu wrote the paper with contributions of all authors.

Acknowledgements:

We would like to thank the DNA cloning, Protein Production, Antibody Production, DNA sequencing facility, tissue culture and mass spectrometry teams of the MRC Protein Phosphorylation and Ubiquitylation Unit for their support. We would like to thank Rosemary Clarke for help with flow cytometry analyses, Sir Philip Cohen for providing reagents, Siamon Gordon for kindly providing MSR1 KO mice, Natalia Shpiro for synthesis of sodium 3-[(2-methyl-2-undecyl-1,3-dioxolan-4-yl)methoxy]-1-propanesulfonate and Carol Clacher, Laura Frew and Gail Gilmour in Transgenic Services for collection of murine femurs. This work was funded by Medical Research Council UK (MC_UU_12016/5) and the pharmaceutical companies supporting the Division of Signal Transduction Therapy (DSTT) (Boehringer-Ingelheim, GlaxoSmithKline and Merck KGaA). We would like to acknowledge Dundee Imaging Facility which is supported by the 'Wellcome Trust Technology Platform' award [097945/B/11/Z] and the 'MRC Next Generation Optical Microscopy' award [MR/K015869/1]. The School of Life Sciences Data Analysis Group and the Flow Cytometry Facility are funded by Wellcome Trust grants 097945/Z/11/Z and 081867/Z/06/Z, respectively.

References

Allavena P, Mantovani A (2012) Immunology in the clinic review series; focus on cancer: tumour-associated macrophages: undisputed stars of the inflammatory tumour microenvironment. Clin Exp Immunol 167: 195-205

Arandjelovic S, Ravichandran KS (2015) Phagocytosis of apoptotic cells in homeostasis. Nat Immunol 16: 907-17

Avci FY, Li X, Tsuji M, Kasper DL (2013) Carbohydrates and T cells: a sweet twosome. Semin Immunol 25: 146-51

Balce DR, Li B, Allan ER, Rybicka JM, Krohn RM, Yates RM (2011) Alternative activation of macrophages by IL-4 enhances the proteolytic capacity of their phagosomes through synergistic mechanisms. Blood 118: 4199-208

Balce DR, Rybicka JM, Greene CJ, Ewanchuk BW, Yates RM (2016) Ligation of FcgammaR Alters Phagosomal Processing of Protein via Augmentation of NADPH Oxidase Activity. Traffic 17: 786-802

Boulais J, Trost M, Landry CR, Dieckmann R, Levy ED, Soldati T, Michnick SW, Thibault P, Desjardins M (2010) Molecular characterization of the evolution of phagosomes. Mol Syst Biol 6: 423

Chanmee T, Ontong P, Konno K, Itano N (2014) Tumor-associated macrophages as major players in the tumor microenvironment. Cancers (Basel) 6: 1670-90

Colegio OR, Chu NQ, Szabo AL, Chu T, Rhebergen AM, Jairam V, Cyrus N, Brokowski CE, Eisenbarth SC, Phillips GM, Cline GW, Phillips AJ, Medzhitov R (2014) Functional polarization of tumour-associated macrophages by tumour-derived lactic acid. Nature 513: 559-63

Desjardins M, Huber LA, Parton RG, Griffiths G (1994) Biogenesis of phagolysosomes proceeds through a sequential series of interactions with the endocytic apparatus. J Cell Biol 124: 677-88

Dill BD, Gierlinski M, Hartlova A, Arandilla AG, Guo M, Clarke RG, Trost M (2015) Quantitative proteome analysis of temporally resolved phagosomes following uptake via key phagocytic receptors. Mol Cell Proteomics 14: 1334-49

Emmerich CH, Ordureau A, Strickson S, Arthur JS, Pedrioli PG, Komander D, Cohen P (2013) Activation of the canonical IKK complex by K63/M1-linked hybrid ubiquitin chains. Proc Natl Acad Sci U S A 110: 15247-52

Fan Y, Yu Y, Shi Y, Sun W, Xie M, Ge N, Mao R, Chang A, Xu G, Schneider MD, Zhang H, Fu S, Qin J, Yang J (2010) Lysine 63-linked polyubiquitination of TAK1 at lysine 158 is required for tumor necrosis factor alpha- and interleukin-1beta-induced IKK/NF-kappaB and JNK/AP-1 activation. J Biol Chem 285: 5347-60

Ghigo E, Barry AO, Pretat L, Al Moussawi K, Desnues B, Capo C, Kornfeld H, Mege JL (2010) IL-16 promotes T. whipplei replication by inhibiting phagosome conversion and modulating macrophage activation. PLoS ONE 5: e13561

Gordon S, Martinez FO (2010) Alternative activation of macrophages: mechanism and functions. Immunity 32: 593-604

Greaves DR, Gordon S (2009) The macrophage scavenger receptor at 30 years of age: current knowledge and future challenges. J Lipid Res 50 Suppl: S282-6

Guo M, Hartlova A, Dill BD, Prescott AR, Gierlinski M, Trost M (2015) High-resolution quantitative proteome analysis reveals substantial differences between phagosomes of RAW 264.7 and bone marrow derived macrophages. Proteomics 15: 3169-74

Hartlova A, Herbst S, Peltier J, Rodgers A, Bilkei-Gorzo O, Fearns A, Dill BD, Lee H, Flynn R, Cowley SA, Davies P, Lewis PA, Ganley IG, Martinez J, Alessi DR, Reith AD, Trost M, Gutierrez MG (2018) LRRK2 is a negative regulator of Mycobacterium tuberculosis phagosome maturation in macrophages. EMBO J 37

Heap RE, Gant MS, Lamoliatte F, Peltier J, Trost M (2017) Mass spectrometry techniques for studying the ubiquitin system. Biochem Soc Trans 45: 1137-1148

Heckmann BL, Boada-Romero E, Cunha LD, Magne J, Green DR (2017) LC3-Associated Phagocytosis and Inflammation. J Mol Biol 429: 3561-3576

Hjerpe R, Aillet F, Lopitz-Otsoa F, Lang V, England P, Rodriguez MS (2009) Efficient protection and isolation of ubiquitylated proteins using tandem ubiquitin-binding entities. EMBO Rep 10: 1250-8

Johnson JL, Newby AC (2009) Macrophage heterogeneity in atherosclerotic plaques. Curr Opin Lipidol 20: 370-8

Kagan JC (2012) Signaling organelles of the innate immune system. Cell 151: 1168-78

Kelley JL, Ozment TR, Li C, Schweitzer JB, Williams DL (2014) Scavenger receptor-A (CD204): a two-edged sword in health and disease. Crit Rev Immunol 34: 241-61

Komohara Y, Takemura K, Lei XF, Sakashita N, Harada M, Suzuki H, Kodama T, Takeya M (2009) Delayed growth of EL4 lymphoma in SR-A-deficient mice is due to upregulation of nitric oxide and interferon-gamma production by tumor-associated macrophages. Cancer Sci 100: 2160-6

Lemke G (2013) Biology of the TAM receptors. Cold Spring Harb Perspect Biol 5: a009076

Lemke G (2017) Phosphatidylserine Is the Signal for TAM Receptors and Their Ligands. Trends Biochem Sci 42: 738-748

Martinez J, Almendinger J, Oberst A, Ness R, Dillon CP, Fitzgerald P, Hengartner MO, Green DR (2011) Microtubule-associated protein 1 light chain 3 alpha (LC3)-associated phagocytosis is required for the efficient clearance of dead cells. Proc Natl Acad Sci U S A 108: 17396-401

Martinez J, Malireddi RK, Lu Q, Cunha LD, Pelletier S, Gingras S, Orchard R, Guan JL, Tan H, Peng J, Kanneganti TD, Virgin HW, Green DR (2015) Molecular characterization of LC3-associated phagocytosis reveals distinct roles for Rubicon, NOX2 and autophagy proteins. Nat Cell Biol 17: 893-906

Murray PJ, Wynn TA (2011) Protective and pathogenic functions of macrophage subsets. Nat Rev Immunol 11: 723-37

Nagata S, Hanayama R, Kawane K (2010) Autoimmunity and the clearance of dead cells. Cell 140: 619-30

Naujoks J, Tabeling C, Dill BD, Hoffmann C, Brown AS, Kunze M, Kempa S, Peter A, Mollenkopf HJ, Dorhoi A, Kershaw O, Gruber AD, Sander LE, Witzenrath M, Herold S, Nerlich A, Hocke AC, van Driel I, Suttorp N, Bedoui S et al. (2016) IFNs Modify the Proteome of Legionella-Containing Vacuoles and Restrict Infection Via IRG1-Derived Itaconic Acid. PLoS Pathog 12: e1005408

Neyen C, Pluddemann A, Mukhopadhyay S, Maniati E, Bossard M, Gordon S, Hagemann T (2013) Macrophage scavenger receptor a promotes tumor progression in murine models of ovarian and pancreatic cancer. J Immunol 190: 3798-805

Piper RC, Dikic I, Lukacs GL (2014) Ubiquitin-dependent sorting in endocytosis. Cold Spring Harb Perspect Biol 6

Platt N, Gordon S (2001) Is the class A macrophage scavenger receptor (SR-A) multifunctional? - The mouse's tale. J Clin Invest 108: 649-54

Podinovskaia M, VanderVen BC, Yates RM, Glennie S, Fullerton D, Mwandumba HC, Russell DG (2013) Dynamic quantitative assays of phagosomal function. Curr Protoc Immunol 102: Unit 14 34

Pulvino M, Liang Y, Oleksyn D, DeRan M, Van Pelt E, Shapiro J, Sanz I, Chen L, Zhao J (2012) Inhibition of proliferation and survival of diffuse large B-cell lymphoma cells by a small-molecule inhibitor of the ubiquitin-conjugating enzyme Ubc13-Uev1A. Blood 120: 1668-77

Ritorto MS, Ewan R, Perez-Oliva AB, Knebel A, Buhrlage SJ, Wightman M, Kelly SM, Wood NT, Virdee S, Gray NS, Morrice NA, Alessi DR, Trost M (2014) Screening of DUB activity and specificity by MALDI-TOF mass spectrometry. Nat Commun 5: 4763

Rothlin CV, Ghosh S, Zuniga EI, Oldstone MB, Lemke G (2007) TAM receptors are pleiotropic inhibitors of the innate immune response. Cell 131: 1124-36

Schultze JL, Schmieder A, Goerdt S (2015) Macrophage activation in human diseases. Semin Immunol 27: 249-56

Sica A, Rubino L, Mancino A, Larghi P, Porta C, Rimoldi M, Solinas G, Locati M, Allavena P, Mantovani A (2007) Targeting tumour-associated macrophages. Expert Opin Ther Targets 11: 1219-29

Stuart LM, Boulais J, Charriere GM, Hennessy EJ, Brunet S, Jutras I, Goyette G, Rondeau C, Letarte S, Huang H, Ye P, Morales F, Kocks C, Bader JS, Desjardins M, Ezekowitz RA (2007) A systems biology analysis of the Drosophila phagosome. Nature 445: 95-101

Tournier C, Dong C, Turner TK, Jones SN, Flavell RA, Davis RJ (2001) MKK7 is an essential component of the JNK signal transduction pathway activated by proinflammatory cytokines. Genes Dev 15: 1419-26

Trost M, English L, Lemieux S, Courcelles M, Desjardins M, Thibault P (2009) The phagosomal proteome in interferon-gamma-activated macrophages. Immunity 30: 143-54

Varin A, Mukhopadhyay S, Herbein G, Gordon S (2010) Alternative activation of macrophages by IL-4 impairs phagocytosis of pathogens but potentiates microbial-induced signalling and cytokine secretion. Blood 115: 353-62

Weavers H, Evans IR, Martin P, Wood W (2016) Corpse Engulfment Generates a Molecular Memory that Primes the Macrophage Inflammatory Response. Cell 165: 1658-1671

Xia ZP, Sun L, Chen X, Pineda G, Jiang X, Adhikari A, Zeng W, Chen ZJ (2009) Direct activation of protein kinases by unanchored polyubiquitin chains. Nature 461: 114-9

Yates RM, Hermetter A, Russell DG (2005) The kinetics of phagosome maturation as a function of phagosome/lysosome fusion and acquisition of hydrolytic activity. Traffic 6: 413-20

Yates RM, Hermetter A, Taylor GA, Russell DG (2007) Macrophage activation downregulates the degradative capacity of the phagosome. Traffic 8: 241-50

Zhang T, Inesta-Vaquera F, Niepel M, Zhang J, Ficarro SB, Machleidt T, Xie T, Marto JA, Kim N, Sim T, Laughlin JD, Park H, LoGrasso PV, Patricelli M, Nomanbhoy TK, Sorger PK, Alessi DR, Gray NS (2012) Discovery of potent and selective covalent inhibitors of JNK. Chem Biol 19: 140-54

Figure legends

Figure 1: Alternative activation affects phagosomal proteolysis and lipolysis but not phagocytosis.

(A-B) Internalization of apoptotic, necrotic Raw 234.7 GFP cells (A), fluorescent negatively charged carboxylated and positively charged amino microspheres (B) in primary M2 (IL-4) and M0 macroophages. Cytochalasin D (6µM) was used as an inhibitor of phagocytosis, 1 h before phagocytosis. Data are shown as means of relative fluorescence units (RFU) ± standard error of the mean (SEM). (C-E) Real-time fluorescence assays for intraphagosomal proteolysis (C), acidification (D) and lipolysis (E) show substantially increased proteolysis, acidification and lipolysis in the phagosomes of M2(IL-4) macrophages. The kinetics of proteolysis, acidification and lipolysis of phagocytosed beads were plotted as a ratio of substrate fluorescence to calibration fluorescence. Beads were added to macrophages at 0 min. Shaded area in (D) & (E) represents SEM. (F) is a representative of three independent experiments. Leupeptin (100nM) and Bafilomycin (100nM) treatment serve as negative controls in (C) and (D), respectively.

Figure 2: Experimental workflow and the phagosome proteome of M2 (IL-4) macrophages.

(A) Workflow of the phagosome proteomics experiment. (B) Volcano plot of the phagosome proteome data. 1,766 proteins were quantified of which 121 proteins were significantly up-regulated and 62 proteins were down-regulated in M2(IL-4) macrophages. Selected proteins are indicated. (C) Heatmap of proteomics data shows high reproducibility between biological replicates. Selected proteins are highlighted. (D-E) Selected Gene Ontology (GO)-terms of biological processes significantly up-regulated (D) and down-regulated (E) on phagosomes of M2(IL-4) macrophages. Selected proteins of these GO-terms are highlighted. Error bars in (D-E) represent standard deviations from three biological replicates.

Figure 3: TAK1/MKK7/JNK complex is recruited to phagosomes of M2 (IL-4) macrophages in a K63 polyubiquitylation-dependent manner.

(A) Immunoblot (IB) analysis showing the recruitment of TAK1, MKK7, JNK and TAB1/TAB2 to the phagosome in M2(IL-4) macrophages, while MKK4 is not recruited. Rab7a, a phagosomal marker, was used as a loading control for phagosomes and vimentin was used as a loading control for total cell lysates. (B) Quantitation of three independent IB experiments for TAK1, MKK7, TAB1 and TAB2 expression on phagosomes of resting M0 macrophages and M2(IL-4) macrophages. Error bars represent SEM. *p<0.01, **p<0.001 (Student's T-test) (C) IB showing enrichment of K63 polyubiquitylated proteins on the phagosome of M2(IL-4) macrophages compared to M0 macrophages. (F) Treatment with the UBC13 inhibitor NSC697923 reduces recruitment of TAB1, TAB2, TAK1 and MKK7 to the phagosome of M2(IL-4) macrophages, indicating a K63-polyubiquitylation dependent translocation for these proteins. (C) and (D) are representatives of three and two independent experiments, respectively.

Figure 4: Phagosomal MSR1 is K63 polyubiquitylated and interacts with Tab1/Tab2/Tak1/MKK7.
(A) Workflow for TUBE pulldown of K63-polyubiquitylated proteins from phagosomal extracts. (B) Selected ubiquitylated phagosomal proteins identified by TUBE-MS approach. (C) Sequences alignment of N-terminal region of murine and human MSR1 shows high sequence identify and conserved ubiquitylated lysine. (D) Tab2-TUBE pull-downs from phagosome extracts of M2(IL-4) macrophages treated with the K63 specific deubiquitylase (DUB) AMSH-LP or the unspecific DUB USP2. (F) MSR1 immunoprecipitation from M2(IL-4) macrophage phagosomes shows that TAB1, TAB2, TAK1 and MKK7 bind to polyubiquitylated MSR1. TAK1 shows a specific pattern of post-translational modifications indicative of its activation. (D-F) are representative of two independent experiments.

Figure 5: MSR1 triggering activates JNK which induces a proinflammatory stimulus.
(A) *Msr1*$^{+/+}$ (WT) and *Msr1*$^{-/-}$ (KO) M0 macrophages and M2(IL-4) macrophages untreated or stimulated with the MSR1 ligands fucoidan or oxLDL (50 µg/ml, 30 min) were analysed for the phosphorylated and the total forms of JNK1/2 and MSR1. ITGAM (CD11b) serves as a loading control. Both fucoidan and oxLDL activate JNK in a MSR1-dependent manner. (B) Immunoblot against MSR1 of TUBE pulldowns of MSR1 WT and KO BMDMs shows increasing amounts of ubiquitylated MSR1 upon alternative activation and further increases upon MSR1 ligation with fucoidan or oxLDL. (C) qPCR data of *Tnfa* and *Il1b* mRNA levels in WT and MSR1 KO M0 and M2(IL-4) BMDMs shows an MSR1-dependent increase of pro-inflammatory cytokines in response to MSR1 ligation by fucoidan. (D) Inhibition of JNK by JNK-IN8 reduces expression of *Tnfa* upon MSR1 ligation, showing that it is JNK-dependent. (E) Flow cytometry analysis of cell surface markers in WT and *MSR1*$^{-/-}$ M0 macrophages and M2(IL-4) macrophages untreated or stimulated with the MSR1 ligands fucoidan (50 µg/ml, 24 h). Data shows MSR1-dependent increase of the early activation markers CD54, CD69 and CD86 and a decrease of the M2 marker CD301b/Mgl2. CD11b serves as a control. Error bars represent SEM. ***p<0.0001; ****p<10^{-5} (Student's T-test) (A-B) Data are representative of three independent experiments.

Figure 6: MSR1 ubiquitylation and JNK activation correlates in human tumour associated macrophages
(A) Immunohistochemistry analysis of MSR1 in patient ovarian, uterus and sarcoma cancers showing tumour-associated macrophages. (B) Pull-downs of K63 polyubiquitin chains and IB analysis of five human primary cancers shows a correlation between the amount of polyubiquitylated MSR1 and JNK activation in an ovarian tumour. (C) Working model: MSR1 is activated by ligation through many different substrates, including apoptotic cells, fucoidan or oxidised LDL (Signal 1). However, only when the macrophage is IL-4-activated (Signal 2) becomes MSR1 ubiquitylated by an unknown E2/E3 ligase. This ubiquitylation recruits Tab2/3, Tak1, Mkk7 and finally JNK, thereby allowing MSR1 to signal directly through the JNK signalling pathway which induces pro-inflammatory gene transcription.

Figure 1

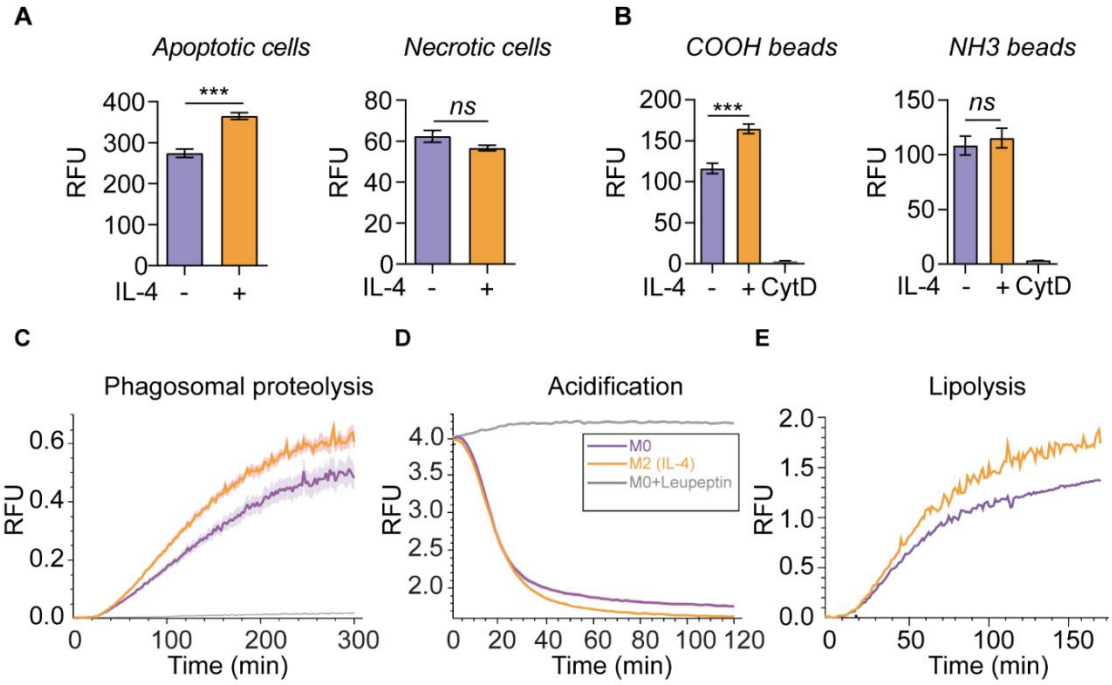

Figure 2

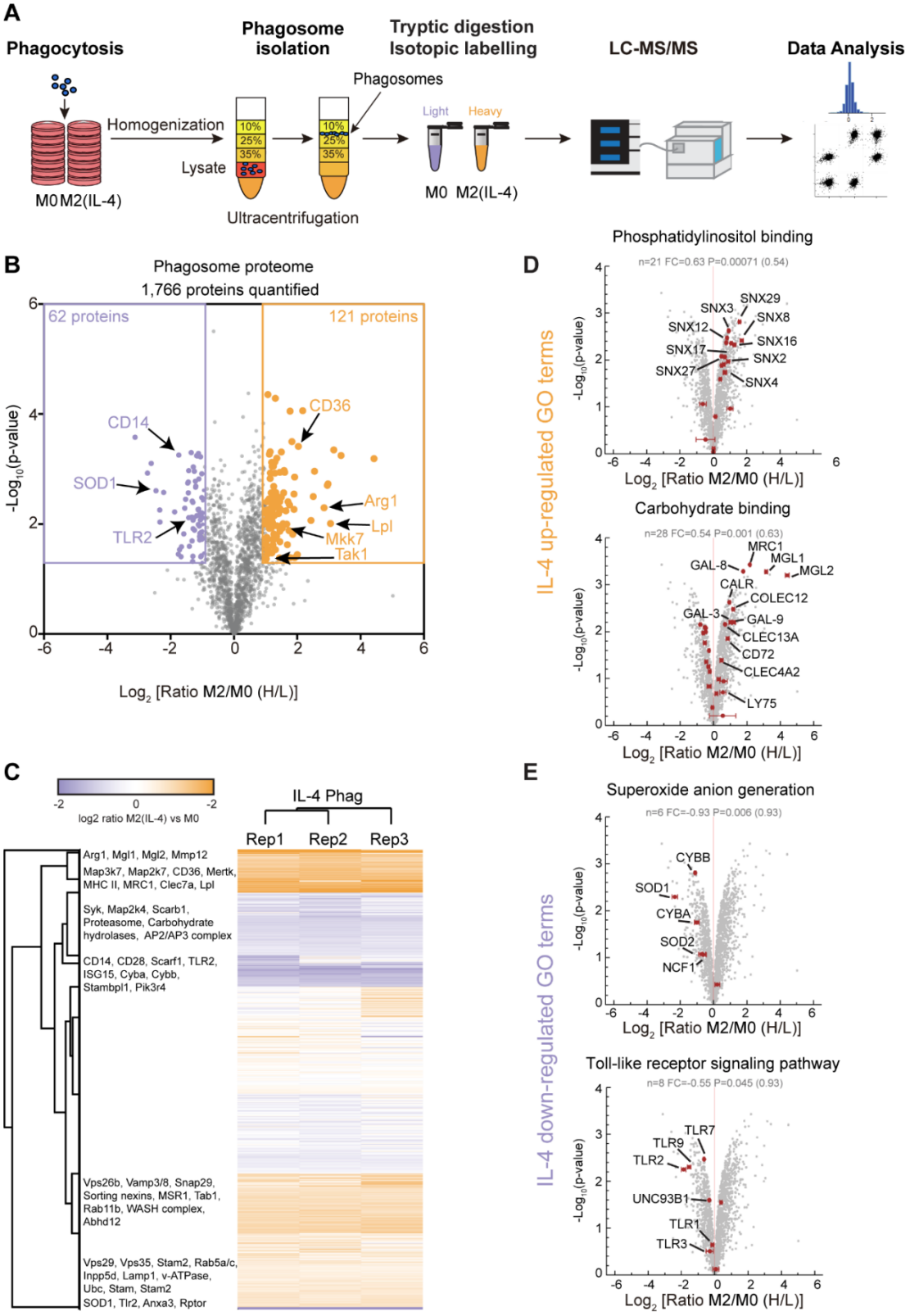

Figure 3

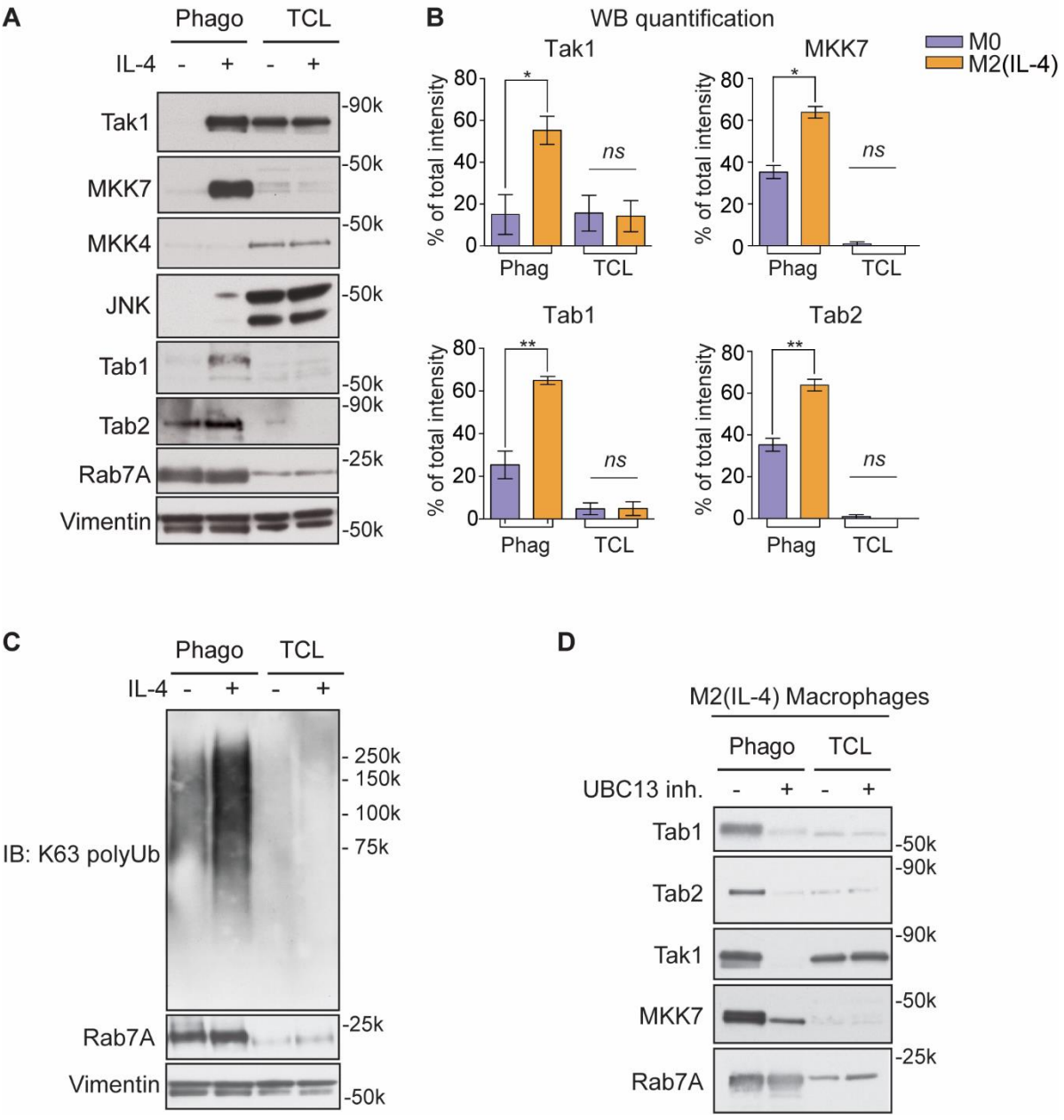

Figure 4

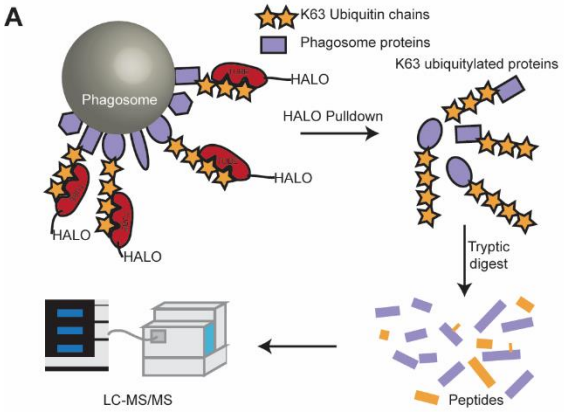

B

Selected ubiquitylated phagosomal proteins identified by TUBE-MS approach

Gene name	Protein	Ubiquitylated position
Ubc	Polyubiquitin-C	63;11;48;1;29;6;27;33
Msr1	Macrophage scavenger receptor 1	27
Slc43a2	Large neutral amino acids transporter small subunit 4	283;293;402;557
Csf1r	Macrophage colony stimulating factor 1 receptor	572;810;625;584
C5ar1	Complement component 5a receptor 1	334
Lyn	Tyrosine-protein kinase Lyn	20
Unc93b1	Protein unc-93 homolog B1	197;582
Lat2	Linker for activation of T cells family member 2	39;84
Abcg1	ATP-binding cassette sub-family G member 1	55
Vamp8	Vesicle-associated membrane protein 8	47
Mgl2	Macrophage galactose N-acetyl-galactosamine	16
Clec4a3	C-type lectin domain family 4 member a3	13
Colec12	Collectin-12	2;17

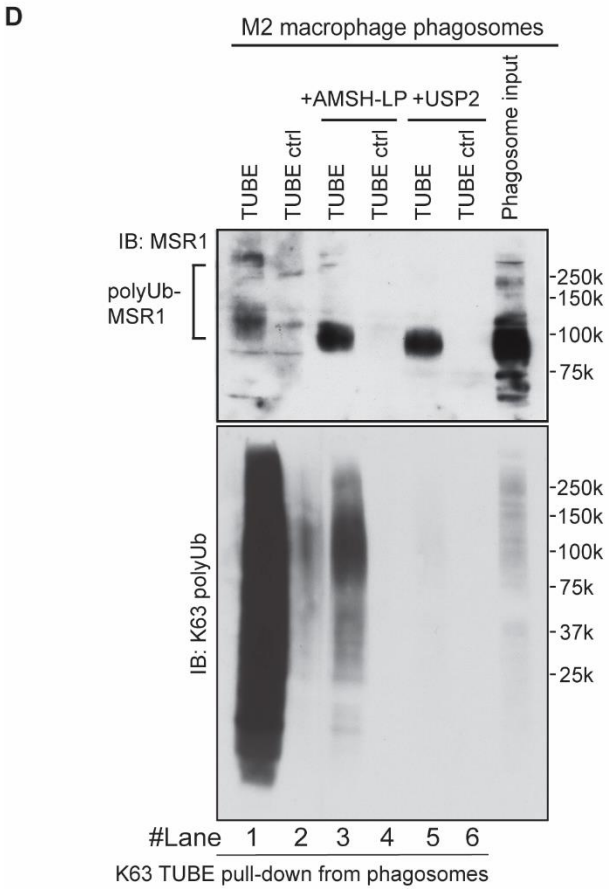

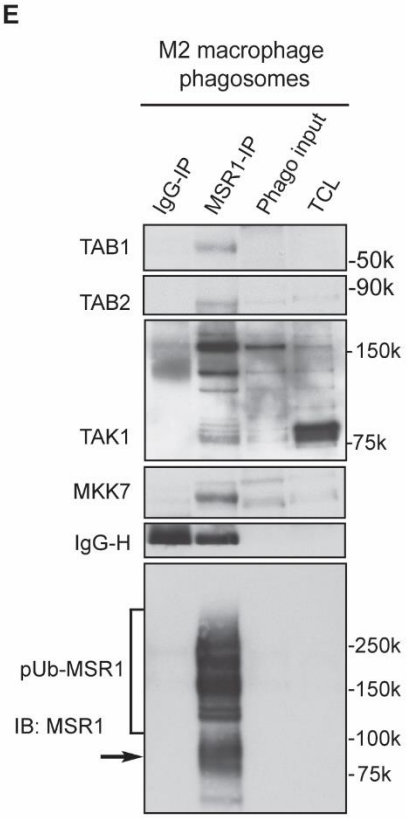

Figure 5: MSR1 activation induces JNK signalling pathway in M2 macrophages

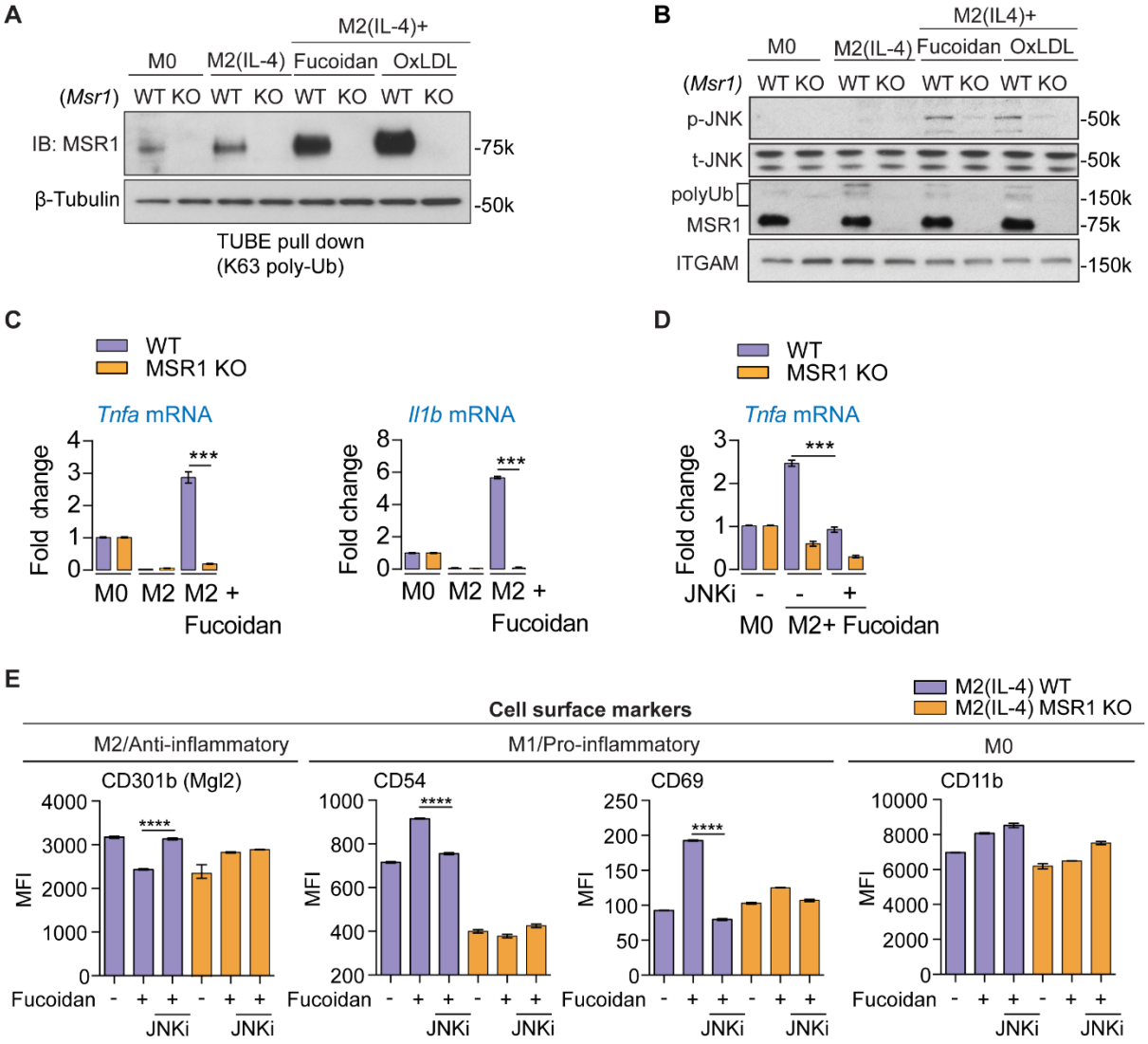

Figure 6